

Experimental study of the Raman strain rosette based on the carbon nanotube strain sensor

Wei Qiu,^a Yi-Lan Kang,^{a*} Zhen-Kun Lei,^b Qing-Hua Qin,^c Qiu Li^a and Quan Wang^b

This work presents a new technique named *Raman strain rosette* for the micro-strain measurement of both Raman active and Raman inactive materials. The technique is based on the theoretical model of the carbon nanotube (CNT) strain sensor that applies the resonance and polarization Raman properties of CNTs and calculates the synthetic contributions of uniformly dispersed CNTs to the entire Raman spectrum. In our work, the proposed technique is applied in different experiments on the Raman inactive materials, such as step-by-step uniaxial tensile and Raman mapping around a circular hole. The experimental results reached by the Raman strain rosette are consistent with the actual values as a whole. This study verifies that the Raman strain rosette is applicable to quantitative measurement of all the in-plane components of the strain tensor (including both normal and shear strains) by three polarized Raman detections for each sampling spot on a microscale. The technique is further applicable to achieving the strain fields through Raman mapping. Copyright © 2010 John Wiley & Sons, Ltd.

Keywords: Raman strain rosette; carbon nanotube strain sensor; Raman inactive; measurement of strain components; polarized Raman spectroscopy

Introduction

Micro-Raman spectroscopy is an effective, precise, noncontact technique with micrometer spatial resolution for strain measurement,^[1] which has been successfully applied in the experimental investigations of, for example, residual and/or intrinsic stresses in silicon-based microsystems,^[2–4] processing stresses in micro/nano films,^[5,6] and interface mechanical behaviors of fiber composites.^[7–9] However, it is noted that the application of Raman strain measurement is restricted to Raman active materials whose spectra have typical and visible Raman modes (peaks) and are sensitive enough to strain.^[8,10] To break such a limitation, some Raman active materials have been applied as strain sensing media. Hitherto, several kinds of Raman active materials have been used as strain sensing media in the mechanical studies of Raman inactive materials and structures, such as aramid fiber,^[11] carbon film,^[12] and poly-p-phenylenebenzobisoxazole (PBO)^[13] and diacetylene-urethane copolymers (DUC) films,^[8] but none has proved to be universally applicable for micro-mechanical measurements.

With the rapid development of manufacturing technology and material property characterization approaches,^[14,15] the carbon nanotube (CNT) has shown the potential to be used as a robust Raman sensor for strain measurements in the micrometer scale.^[16,17] This is due to its outstanding mechanical^[15,18] and spectral properties such as high sensitivity to axial deformation^[19,20] as well as resonant and polarized Raman effects.^[21,22] Wagner and coworkers^[23–26] introduced two methods to realize that idea: the nonpolarized Raman for oriented CNTs and the polarized Raman for stochastic CNTs. The former method was applicable for measuring the strain (actually the normal strain component) in the unique direction along which the CNTs are well oriented. The latter was proposed to detect the strain in any direction by observing the Raman shift increment obtained in the polarization direction (PD) parallel to that of the detected normal strain. Using these methods, Zhao and Wagner^[26] studied the stress concentration around

a fiber end inside a polymer matrix. Frogley *et al.*^[27] and Zhao *et al.*^[28] analyzed the material properties of rubber composites. Nevertheless, the previous methods of using CNTs as strain sensors are approximate and can only be used under certain conditions for strain measurement. Furthermore, there appears to be a lack of a universal and accurate technique applicable to detect strain, and even all the strain components, in Raman inactive materials using Raman sensors.

This work presents a new technique named the *Raman strain rosette* that can be used to measure all the in-plane strain components (including normal and shear strains). The so-called Raman strain rosette is based on the theoretical model of the CNT strain sensor which calculates the synthetic contributions of uniformly dispersed CNTs to the entire Raman spectrum. In our work, the proposed technique is applied in different experiments, such as step-by-step uniaxial tensile and Raman mapping around a circular hole, to Raman inactive materials. Both the validity and the practicability of the Raman strain rosette are verified by comparing the experimental results given by Raman strain rosette with the actual strain values.

* Correspondence to: Yi-Lan Kang, Department of Mechanics, Tianjin University, 300072 Tianjin, P. R. China. E-mail: qiuwei_tju@hotmail.com

a Department of Mechanics, Tianjin University, 300072 Tianjin, P. R. China

b State Key Laboratory of Structural Analysis for Industrial Equipment, Department of Engineering Mechanics, Dalian University of Technology, Dalian 116024, P. R. China

c Department of Engineering, Australian National University, Canberra ACT 2601, Australia

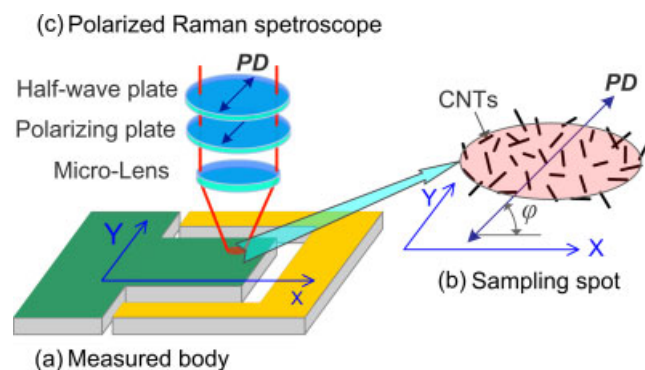


Figure 1. Diagrammatic sketches of CNT strain sensors by polarized Raman spectroscopy. (a) Measured body, (b) CNTs dispersed uniformly and stochastically on the surface of the measured body, (c) polarized Raman spectroscope.

Theoretical Model and Technique

The theoretical model of CNT strain sensor by Raman spectroscopy can be described as follows.^[29] A solid body in a Cartesian coordinate system is measured by a polarized Raman spectroscope in the backscattering geometry with a PD φ as shown in Fig. 1(a). The surface of the body is attached with CNTs randomly but uniformly, as shown in Fig. 1(b), so that the CNTs deform together with the body. The relationship between Raman shift increment of a random individual CNT and the three in-plane strain components is given as Eqn (1):

$$\begin{aligned} \Delta\omega(\theta) &= \Psi_{\text{Sensor}} \cdot \varepsilon(\theta) \\ &= \Psi_{\text{Sensor}} \cdot (\varepsilon_X \cos^2 \theta + \varepsilon_Y \sin^2 \theta - \gamma_{XY} \cos \theta \sin \theta) \end{aligned} \quad (1)$$

where θ is the axial direction (AD) of the nanotube; $\Delta\omega(\theta)$ is denoted as the Raman shift increment of an individual CNT in the AD in θ ; ε_X , ε_Y , and γ_{XY} are the normal strains in the X and Y directions and shear strain, respectively, and Ψ_{Sensor} is defined as strain to Raman shift coefficient of the CNT sensor.

In the Raman test, the spectrum obtained from the surface of the measured body by the polarized Raman spectroscope (Fig. 1(c)) is the summation of the Raman data of all the individual CNTs inside the sampling spot. By applying the statistical properties of the Cauchy/normal distribution, the analytical relationship between the Raman shift increment of the spectrum from all the CNTs and the three in-plane strain components at the sampling point is

$$\begin{aligned} \Delta\Omega(\varphi) &= \frac{\int_{-\pi/2}^{\pi/2} \Delta\omega(\theta) \cdot R(\theta - \varphi) d\theta}{\int_{-\pi/2}^{\pi/2} R(\theta - \varphi) d\theta} \\ &= \frac{\int_{-\pi/2}^{\pi/2} \Psi_{\text{Sensor}} \cdot (\varepsilon_X \cos^2 \theta + \varepsilon_Y \sin^2 \theta - \gamma_{xy} \cos \theta \sin \theta) \cdot R(\theta - \varphi) d\theta}{\int_{-\pi/2}^{\pi/2} R(\theta - \varphi) d\theta} \end{aligned} \quad (2)$$

where R is the scattering intensity of the G' band of an individual nanotube. Actually, R is a function of the angle between the AD and PD, $(\theta - \varphi)$, owing to the polarized Raman properties of CNTs.^[21,22]

Equation (2) represents the general mathematical model of the CNT strain sensor. It is reasonable to simplify such a complex

Table 1. The measured results by the Raman strain rosette and their respective actual values

Specimen		Ψ_{Sensor} (cm^{-1})	ν	$\gamma_{XY}/\varepsilon_X$
A	Measurement result	-1815.0	0.372	0.033
	Actual value	-	0.379	0
B	Measurement result	-1812.5	0.332	0.041
	Actual value	-	0.330	0

expression to reach a more applicable form in accordance with the actual modes of Raman experiments.^[30,31] For instance, when the PDs of the incident and scattered lights are arranged to be constantly parallel to each other (as shown in Fig. 1(c)), the polarized Raman scattering of CNTs is in its resonant state and behaves as an antenna effect; $R = \kappa \cos^4(\theta - \varphi)$ and $\kappa = \text{const.}$ ^[30] Hence, Eqn (2) can be simplified as

$$\begin{aligned} \Delta\Omega(\varphi) &= \frac{1}{6} \Psi_{\text{Sensor}} \cdot [(3 + 2 \cos 2\varphi)\varepsilon_X + (3 - 2 \cos 2\varphi)\varepsilon_Y \\ &\quad - 2 \sin 2\varphi \cdot \gamma_{XY}] \end{aligned} \quad (3)$$

Equation (3) indicates that the Raman shift increment achieved in any given PD can be expressed by a linear combination of three in-plane strain components with different trigonometric functions relative to the PD as weighted parameters. Therefore, for three different PDs, three equations are written to form a set of simultaneous equations as follows. In particular, when the PDs are set as $0^\circ/45^\circ/90^\circ$ to the X -axis, we have

$$\begin{cases} \varepsilon_X = \frac{1}{4\Psi_{\text{Sensor}}} \cdot (5\Delta\Omega^{(0)} - \Delta\Omega^{(90)}) \\ \varepsilon_Y = \frac{1}{4\Psi_{\text{Sensor}}} \cdot (5\Delta\Omega^{(90)} - \Delta\Omega^{(0)}) \\ \gamma_{XY} = \frac{3}{2\Psi_{\text{Sensor}}} \cdot (\Delta\Omega^{(0)} + \Delta\Omega^{(90)} - 2\Delta\Omega^{(45)}) \end{cases} \quad (4)$$

With Eqn (4), we present the following measurement procedures for the new Raman strain rosette technique for strain measurement. Take the 45° Raman strain rosette as an example. First, a CNT film is prepared on the surface of the body to be measured by means of self-assembly, printing or pasting, etc. In the next step, the Ψ_{Sensor} is calibrated through experiments. The Raman spectra in three PDs $0^\circ/45^\circ/90^\circ$ are then detected through polarized Raman tests to determine the Raman shifts, which are in turn substituted into Eqn (4) to finally obtain ε_X , ε_Y , and γ_{XY} . By further applying Hooke's law, the mechanical parameters including the stress components, principal strain, and principal stress also become obtainable.

Specimens and Experiments

The work presented in this paper involve several uniaxial tensile tests applying the Raman strain rosette, which were preformed on Specimens A, B, and C.

Specimen A: freestanding CNT film

The matrix material was a diglycidyl ether of bisphenol-A (DGEBA)-based epoxy. Single-walled carbon nanotubes (SWNTs) functionalized by $-\text{COOH}$ group (0.5 wt%, TIMESNANO Ltd.) were dispersed in a liquid epoxy by ultrasonication for 24 h and hardener (25 wt%) was

mixed in, followed by vacuum pumping to remove air bubbles at 80 °C. The mixture was dropped on a quartz plate and then covered with another quartz plate. The top plate was then pressed slowly, which produced a film of about 160 μm thickness. The film was then left for curing at 80 °C for 6 h before cooling down to room temperature in air. The cured film was peeled from the quartz plates carefully and cut into strips of about 40 × 2 mm² in size. Young's modulus and Poisson's ratio of the film were measured to be 2.00 GPa and 0.379, respectively.

Specimen B: PVC sheet coated by a CNT film

The polyvinyl chloride(PVC) sheet is about 400 μm thick and has a Young's modulus of 1.34 GPa and Poisson's ratio of 0.330. The CNT film was prepared on the PVC sheet following a similar approach as was used for specimen A. The film obtained was about 30 μm thick, which is much thinner than its substrate. Specimen B was also cut to strips of 40 mm × 2 mm in size.

Specimen C: PVC sheet with a circular hole and coated by a CNT film

A PVC sheet similar to Specimen B was cut to the shape as shown in Fig. 2(a). A circular hole was punched in the middle of the dog-bone-shaped sample. A CNT film of 30 μm thickness was prepared on the PVC surface.

The specimens were tested in a mini-tensile machine (Fig. 3) with the loading direction (X-direction) parallel to the longitudinal axis of each specimen. The freestanding CNT film was loaded in steps of 0.4% strain when $\epsilon_x < 0.72\%$ and 0.2% when $\epsilon_x \geq 0.72\%$ until the sample reached final rupture. Specimen B was also loaded stepwise at about 0.17% strain per step until ϵ_x reached 0.29%. A Renishaw InVia Raman spectroscope with a He-Ne laser source (632.8 nm, 2 mW) was utilized and the incident beam was focused on the CNT film surface of each specimen in the backscattering geometry through a 50× objective lens, forming a sampling spot of about 2 μm in diameter. For each loading step, a 45° Raman strain rosette was employed to record the Raman spectra at the

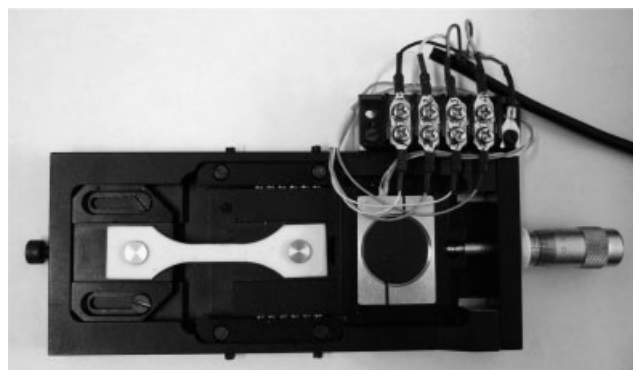


Figure 3. Photograph of the mini-tensile machine.

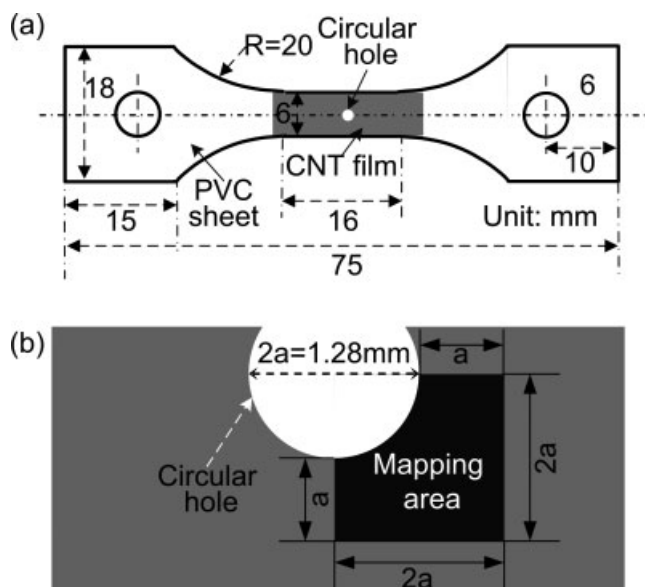


Figure 2. Diagrammatic sketches of Specimen C. (a) Geometrical shape and dimensions, (b) Raman mapping region.

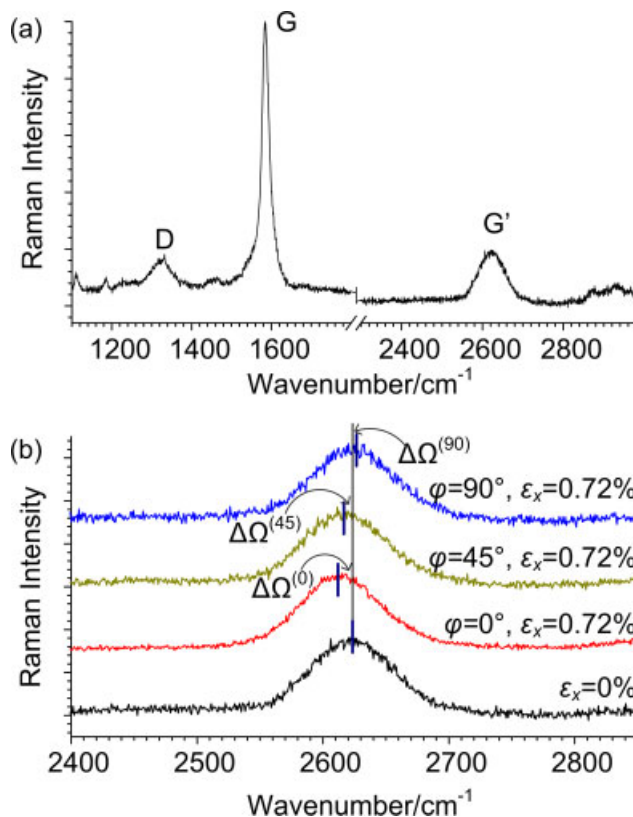


Figure 4. (a) A Raman spectrum detected from CNT/epoxy film. (b) G' band spectra with different loading and polarization directions.

same sampling spot from 2450 to 2800 cm⁻¹ (G' band region) in 0°/45°/90° PDs, respectively. In testing Specimen C, the sheet was loaded uniaxially to 0.33% average strain around the middle of the dog-bone sample. After waiting for 1 h for stress relaxation, a quarter area around the hole (Fig. 3(b)) was scanned by the same Raman system using 60 μm mapping steps. In each of the sampling spots during Raman mapping, 45° Raman strain rosette was applied.

Results and Discussion

Figure 4(a) shows a Raman spectrum detected from the SWNT/epoxy film in our test. In this spectrum, the typical modes of CNT are sufficiently discernible, such as the D band at about

1300 cm⁻¹, the G band at about 1600 cm⁻¹, and the G' band at about 2600 cm⁻¹. As for the G' band, it is well known that both epoxy and PVC are Raman inactive to strain and show no visible mode between 2450 and 2800 cm⁻¹. Thus, the fluorescence-removed Raman data near the G' band can be regarded as totally coming from the CNTs inside the matrix and/or on the substrate. The data can be fitted by a Lorentz/Gauss function to achieve the actual location of G' band (viz. Raman shift). Furthermore, when the sample is under loading, the G' band will move upward or downward as shown in Fig. 4(b). The increments of the Raman shifts are quite dissimilar when the samples are under the same loading but with different PDs of Raman system.

Figure 5(a) shows the variation of G' Raman shift during the uniaxial tensile test on the freestanding CNT film. It can be seen that the Raman shifts in all the PDs ($\Omega^{(0)}$, $\Omega^{(45)}$, and $\Omega^{(90)}$) start from about 2624 cm⁻¹, vary linearly with the increase of tensile load until $\varepsilon_X \geq 0.8\%$, and then nonlinearly before the film breaks. The slopes of Raman shift variations in the linear range, $\Delta\Omega^{(0)}/\varepsilon_X$, $\Delta\Omega^{(45)}/\varepsilon_X$, and $\Delta\Omega^{(90)}/\varepsilon_X$, are -14.0, -5.9, and 2.6, respectively. Dividing both sides by ε_X for each equation in Eqn (4) and substituting the Raman shift slopes as given by Fig. 5(a) and the respective PDs, we obtain

$$\begin{cases} 1 = \frac{1}{4\Psi_{\text{Sensor}}} \cdot \left(5 \frac{\Delta\Omega^{(0)}}{\varepsilon_X} - \frac{\Delta\Omega^{(90)}}{\varepsilon_X} \right) \Rightarrow \Psi_{\text{Sensor}} \\ \quad = -1815 \text{ cm}^{-1} \\ \frac{\varepsilon_Y}{\varepsilon_X} = \frac{1}{4\Psi_{\text{Sensor}}} \cdot \left(5 \frac{\Delta\Omega^{(90)}}{\varepsilon_X} - \frac{\Delta\Omega^{(0)}}{\varepsilon_X} \right) \Rightarrow \nu = -\frac{\varepsilon_Y}{\varepsilon_X} = 0.372 \quad (5) \\ \frac{\gamma_{XY}}{\varepsilon_X} = \frac{3}{2\Psi_{\text{Sensor}}} \cdot \left(\frac{\Delta\Omega^{(0)}}{\varepsilon_X} + \frac{\Delta\Omega^{(90)}}{\varepsilon_X} - 2 \frac{\Delta\Omega^{(45)}}{\varepsilon_X} \right) \\ \quad = 0.033 \longrightarrow 0 \end{cases}$$

Equation (5) shows that the experimentally measured strains are quite consistent with their respective theoretical counterparts (as Table 1 listed). For instance, the Poisson's ratio obtained by Raman strain rosette, 0.372, is almost equal to its actual value of 0.379. The measured shear strain in the X-Y direction, which is nearly zero, may be due to some experimental uncertainty. The strain to Raman shift coefficient of the CNT sensor (Ψ_{Sensor}) is obtained as -1815 cm⁻¹.

Figure 5(b) gives the experimental data of the test on Specimen B, which shows that $\Omega^{(0)}$, $\Omega^{(45)}$, and $\Omega^{(90)}$ are also varying linearly. By processing the slopes of Raman shift distributions in a similar way following Eqn (5), we obtained a Poisson's ratio of 0.335 which is very close to the actual value of 0.330 for PVC. It is noted that the measured value should be very close to the Poisson's ratio of PVC but different from 0.379 of the CNT film since the film is far thinner than the PVC substrate. The obtained shear strain is near zero (as Table 1 listed), too. Besides, the Ψ_{Sensor} of coated CNT film is very close to that of freestanding CNT film, which is reasonable because both films are made of the same material and prepared with the same method.

The Raman shift data of the test on the PVC sheet with a micro-hole coated by a CNT film were substituted into Eqn (4) to obtain the distributions of strain components in the quarter area around the hole. Three strain components were then transformed to stress components in the Cartesian coordinate system by applying the generalized Hooke's law given in Eqn (6) below.

$$\begin{cases} \sigma_X = \frac{E}{1-\nu^2}(\varepsilon_X + \nu\varepsilon_Y) \\ \sigma_Y = \frac{E}{1-\nu^2}(\varepsilon_Y + \nu\varepsilon_X) \\ \tau_{XY} = \frac{E}{2(1+\nu)}\gamma_{XY} \end{cases} \quad (6)$$

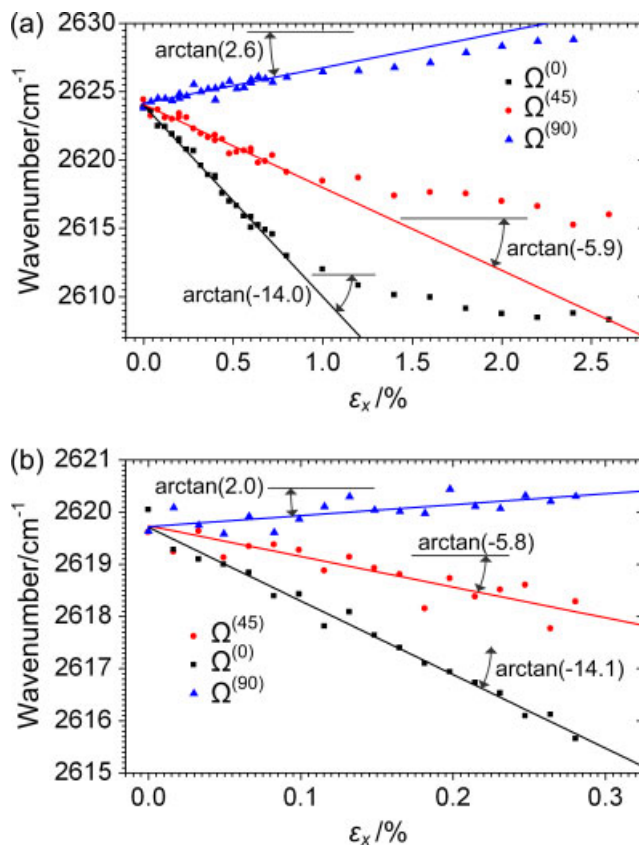


Figure 5. Experimental data of the Raman tests on (a) Specimen A and (b) Specimen B.

The polar components are calculated through coordinate conversion as follows:

$$\begin{cases} \sigma_r = \frac{\sigma_X + \sigma_Y}{2} + \frac{\sigma_X - \sigma_Y}{2} \cos 2\theta - \tau_{XY} \sin 2\theta \\ \sigma_\theta = \frac{\sigma_X + \sigma_Y}{2} - \frac{\sigma_X - \sigma_Y}{2} \cos 2\theta + \tau_{XY} \sin 2\theta \\ \tau_{r\theta} = \frac{\sigma_X - \sigma_Y}{2} \sin 2\theta + \tau_{XY} \cos 2\theta \end{cases} \quad (7)$$

The obtained distributions of stress components in polar coordinate system, σ_r , σ_θ , and $\tau_{r\theta}$, are as shown in Fig. 6(a)–(c), respectively. Their theoretical solutions^[32] are given in Fig. 6(d)–(f), respectively. It can be seen that the results achieved by Raman strain rosette are similar to their theoretical counterparts in both trend and the magnitude. In detail, σ_θ shows an apparent stress concentration near the lateral rim of the hole and the so-obtained stress concentration factor, 2.66, approaches its theoretical value of 3. Meanwhile, the measured distribution of $\tau_{r\theta}$ shows a clear saddle-shaped appearance and symmetric about a line along $\theta = 45^\circ$. From the area along the 45° line to the areas near X- and Y-axes, the sign of the shear strain alters from negative to positive and the magnitude changes sharply in the areas near X- and Y-axes. Actually, the direct measurement of $\tau_{r\theta}$ distribution in microscale is almost impossible by most of the experimental mechanics methods.

Conclusions

In this work, an experimental study on a new technique of strain measurement named Raman strain rosette is proposed.

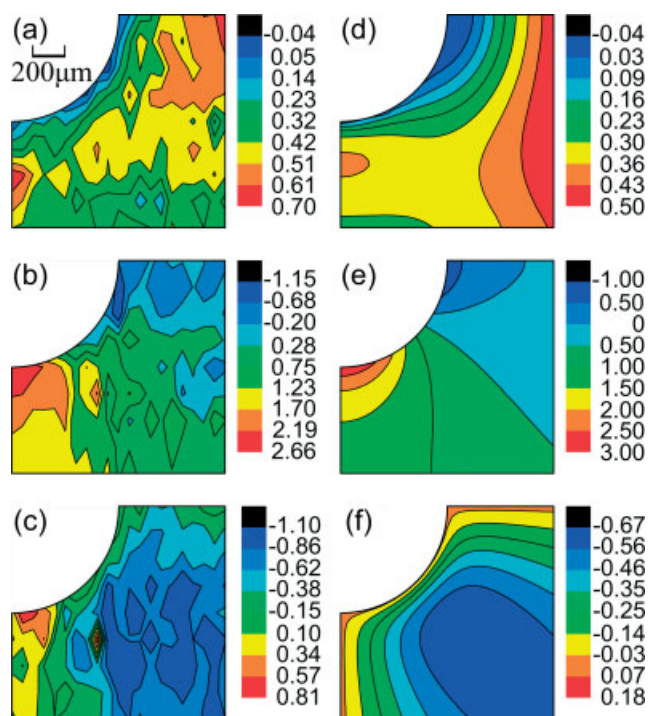


Figure 6. The distributions of stress components around the circular hole of Specimen C. (a)–(c), σ_{rr} , $\sigma_{\theta\theta}$, and $\tau_{r\theta}$ achieved by the Raman strain rosette, respectively. (d)–(f), σ_{rr} , $\sigma_{\theta\theta}$, and $\tau_{r\theta}$ given by elastic mechanics theory, respectively.

By means of polarized Raman spectroscopy the technique is applicable to measure in-plane strains with micrometer spatial resolution of both Raman active and Raman inactive materials/structures. The technique originates from the theoretical model of carbon nanotube strain sensor, which formulates the analytical relationship between the polarized Raman spectrum of uniformly dispersed CNTs and the in-plane strain components via calculating the synthetic contributions from individual CNTs in random directions to the entire Raman spectrum. The proposed technique is applied in several experiments to the Raman inactive materials, such as step-by-step uniaxial tensile and Raman mapping around a circular hole. The experimental results reached by the Raman strain rosette are consistent with the actual values on the whole. This study verifies that the Raman strain rosette is applicable to quantitative measurement of all the in-plane components of the strain tensor (including both normal and shear strains) by three polarized Raman detections for each sampling spot. The technique is further applicable to achieving the strain fields through Raman mapping.

Acknowledgement

This work is funded by the National Natural Science Foundation of China (No. 10732080 and No. 10972047).

References

- [1] V. T. Srikar, S. M. Spearing, *Exp. Mech.* **2003**, *43*, 238.
- [2] I. De Wolf, *J. Raman Spectrosc.* **1999**, *30*, 877.
- [3] I. De Wolf, C. Jian, W. M. van Spengen, *Opt Lasers Eng.* **2001**, *36*, 213.
- [4] Y. L. Kang, Y. Qiu, Z. K. Lei, M. Hu, *Opt Lasers Eng.* **2005**, *43*, 847.
- [5] W. Qiu, Y. L. Kang, Q. Li, Z. K. Lei, Q. H. Qin, *Appl. Phys. Lett.* **2008**, *92*, 041906.
- [6] P. S. Dobal, R. S. Katiyar, *J. Raman Spectrosc.* **2002**, *33*, 405.
- [7] M. S. Amer, L. S. Schadler, *J. Raman Spectrosc.* **1999**, *30*, 919.
- [8] R. J. Young, C. Thongpin, J. L. Stanford, P. A. Lovell, *Composites Part A*. **2001**, *32*, 253.
- [9] Z. K. Lei, W. Qiu, Y. L. Kang, L. Gang, H. Yun, *Composites Part A*. **2008**, *39*, 113.
- [10] A. C. Ferrari, J. Robertson, *Raman Spectroscopy in Carbons: from Nanotubes to Diamond*, The Royal Society: London, **2004**.
- [11] J. Parthenios, D. G. Katerelos, G. C. Psarras, C. Galiotis, *Eng. Fract. Mech.* **2002**, *69*, 1067.
- [12] C. A. Taylor, M. F. Wayne, W. K. S. Chiu, *Thin Solid Films*. **2003**, *429*, 190.
- [13] H. Miyagawa, C. Sato, K. Ikegami, *Composites Part A*. **2001**, *32*, 477.
- [14] H. J. Dai, *Acc. Chem. Res.* **2002**, *35*, 1035.
- [15] M. Terrones, *Annu. Rev. Mater. Res.* **2003**, *33*, 419.
- [16] C. A. Cooper, R. J. Young, *J. Raman Spectrosc.* **1999**, *30*, 929.
- [17] J. R. Wood, Q. Zhao, M. D. Frogley, E. R. Meurs, A. D. Prins, T. Peijs, D. J. Dunstan, H. D. Wagner, *Phys. Rev. B*. **2000**, *62*, 7571.
- [18] E. T. Thostenson, Z. F. Ren, T. W. Chou, *Compos. Sci. Technol.* **2001**, *61*, 1899.
- [19] C. C. Kao, R. J. Young, *Compos. Sci. Technol.* **2004**, *64*, 2291.
- [20] S. B. Cronin, A. K. Swan, M. S. Unlu, B. B. Goldberg, M. S. Dresselhaus, M. Tinkham, *Phys. Rev. B*. **2005**, *72*, 035425.
- [21] M. S. Dresselhaus, G. Dresselhaus, R. Saito, A. Jorio, *Phys. Rep. Rev. Sect. Phys. Lett.* **2005**, *409*, 47.
- [22] G. S. Duesberg, I. Loa, M. Burghard, K. Syassen, S. Roth, *Phys. Rev. Lett.* **2000**, *85*, 5436.
- [23] Q. Zhao, J. R. Wood, H. D. Wagner, *Appl. Phys. Lett.* **2001**, *78*, 1748.
- [24] Q. Zhao, M. D. Frogley, H. D. Wagner, *Compos. Sci. Technol.* **2002**, *62*, 147.
- [25] M. D. Frogley, Q. Zhao, H. D. Wagner, *Phys. Rev. B*. **2002**, *65*, 113413.
- [26] Q. Zhao, H. D. Wagner, *Composites Part A*. **2003**, *34*, 1219.
- [27] M. D. Frogley, D. Ravich, H. D. Wagner, *Compos. Sci. Technol.* **2003**, *63*, 1647.
- [28] Q. Zhao, R. Tannenbaum, K. J. Jacob, *Carbon*. **2006**, *44*, 1740.
- [29] W. Qiu, Y.-L. Kang, Z.-K. Lei, Q.-H. Qin, Q. Li, *Chin. Phys. Lett.* **2009**, *26*, 080701.
- [30] H. H. Gommans, J. W. Alldredge, H. Tashiro, J. Park, J. Magnuson, A. G. Rinzier, *J. Appl. Phys.* **2000**, *88*, 2509.
- [31] R. Saito, G. Dresselhaus, M. S. Dresselhaus, *Physical Properties of Carbon Nanotubes*, Imperial College Press: London, **1998**.
- [32] A. E. H. Love, *A Treatise on the Mathematical Theory of Elasticity* (4th edn), Dover Publications: New York, **1944**.